Thin-Walled Structures 59 (2012) 171–180

Contents lists available at SciVerse ScienceDirect

Thin-Walled Structures

journal homepage: www.elsevier.com/locate/tws

Finite element buckling analysis of stiffened plates with filleted junctions

Patrick E. Fenner, Andrew Watson *

Automotive and Aeronautical Engineering Department, Loughborough University, Loughborough, Leicestershire, LE11 3TU, UK

ARTICLE INFO

Article history:
Received 10 October 2011
Received in revised form
15 May 2012
Accepted 23 May 2012
Available online 10 July 2012

Keywords:
Fillet junctions
Buckling
Finite element
Postbuckling
VICONOPT

ABSTRACT

Modern aircraft wings are thin-walled structures composed of ribs, spars and stiffened panels, where the top skin is subject to compressive forces in flight that can cause buckling instability. If these panels are machined from a single billet of metal then the initial buckling performance can be significantly improved by increasing the fillet radius along the line junction between the stiffener webs and skin. Typically thin-walled structures are usually modelled with two dimensional elements. To model the stiffened panel with fillets three dimensional elements are required. For the stiffened panel selected for the analysis the paper shows that the three dimensional model shows a substantial increase in skin initiated buckling if the fillet is taken account of. A 5 mm radius leads to an increase of 34% increase in local buckling load performance for a skin portion of breath to thickness ratio of 100. The associated overall buckling load increases by 1.8%. The mass penalty for a 5 mm radius is 5.1%. To avoid local and overall buckling interaction an accurate measure of both buckling loads is very important and may have impact for designers. The three dimensional models with no fillets show very good agreement with the two dimensional models.

1. Introduction

Aircraft structural systems are thin-walled structures with wing structure composed of ribs, spars and stiffened panels. For civil aircraft, the top skin is, under aerodynamic loading, subject to axial compressive forces that can cause buckling instability. Typically these stiffened panels can have a considerable postbuckling reserve of strength, enabling them to remain in stable equilibrium under loads in excess of their critical buckling load, provided the initial buckling mode is a local one [1].

Aircraft wing components and fuselage components are joined, in metallic structure, by means of riveting (and more recently welding) to form complete wing and fuselage structure. For stiffened panel construction components can be machined integrally. Single piece stiffened panels have several potential advantages that include cost savings through reductions in assembly labour, tooling, part count and manufacturing time [2,3].

This paper investigates the influence on the buckling performance of a stiffened panel caused by variation in the cross sectional geometry of the line junctions between the component plates that form the cross section of the stiffened panel. It is assumed that the stiffened panel is machined from a single billet of aluminium and that there is a fillet radius at each line junction of component plates i.e. the stiffener webs and inter-stiffener portions of skin. The comparison of the line junction geometry between a filleted and non-filleted junction (or square as it is termed in this paper for distinction) is shown in Fig. 1. A range of fillet radii are analysed. In a previous study only one fillet was analysed [4]. The buckling analysis is restricted to local and overall buckling only.

Classical and non-classical boundary conditions have been investigated by other authors [5–8]. ESDU data item 72019 [5] investigates the buckling of flat isotropic plates under uniaxial loading with simply supported edges with different degrees of elastic restraint, in rotation, on the longitudinal edges. For plates with one longitudinal edge free and the other longitudinal edge elastically restrained, in rotation, results are presented in NACA technical report 734 [6]

The Computer Numerical Control (CNC) machining does allow for very low tolerance values i.e. $\ll 1$ mm and near square junctions are possible from this manufacturing process. The designer has to assess whether the performance gains are beneficial when compared to the heavier mass panels caused by the extra material present in a filleted junction panel.

The larger the radius of the fillet: the heavier the panel becomes. The geometry of the fillet then becomes a design constraint which affects the mass optimisation of the panel. The choice of fillet radii also influences durability and damage tolerance considerations [9]. Riveted panels have crack arresting features due to discontinuities in the structural form. There is research however that shows crack panel durability can be improved by introducing buckling containment features such as

* Corresponding author.
E-mail address: a.watson@lboro.ac.uk (A. Watson).

0263-8231
http://dx.doi.org/10.1016/j.tws.2012.05.011

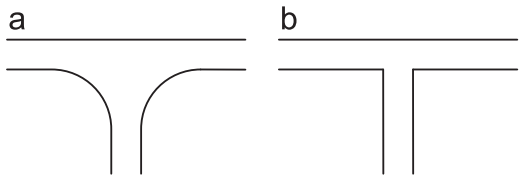

Fig. 1. Line junction geometry: (a) filleted junction and (b) square junction.

skin crenulations or stiffener pad-ups [10]. These panels are continuous systems from integrally machined panels and the containment features significantly influence the fatigue crack growth performance of the stiffened panel.

The stiffened panel used in the investigation comes from work originated by NASA into the buckling loads of stiffened panels subjected to combined in plane loadings. The fillet radii values were based on this stiffened panel and fillet values, in the range 1–5 mm, were chosen. This selection of values caused variation in the buckling performance of the stiffened panel. For typical aerospace panels, larger values of fillet radii are normal.

An optimum stiffened panel typically results in the critical buckling stress occurring with a skin mode and a higher buckling stress for the overall mode. At any bifurcation point there will be a redistribution of stresses and a growth in out-of-plane deflection resulting in a reduction in the stiffness of the whole section. Hence when local buckling occurs the overall buckling stress will reduce further and so it is important that there is a significant difference in the initial and overall buckling loads for the panel to ensure postbuckling stability [11] This paper only examines the initial buckling performance but the work presented does have implications for the optimisation of stiffened panels with a postbuckled reserve of strength.

Analytical and numerical buckling results are presented in this paper. Analytical results are obtained with the computer programme VICONOPT [12]. Numerical results are obtained using the Finite Element programme MSC NASTRAN (v2007.1) [13] using the MSC PATRAN (2010.2.3 64-Bit) pre-processor. The results presented use VICONOPT to compute flat plate and square junction buckling results only. Square junction and filleted junction results are obtained using NASTRAN.

2. VICONOPT background

VICONOPT (VIPASA with CONstraints and OPTimisation) [12] is a FORTRAN 77 computer programme that incorporates the earlier programs VIPASA (Vibration and Instability of Plate Assemblies including Shear and Anisotropy) [14] and VICON (VIPASA with CONstraints) [15]. It covers any prismatic plate assembly, that is panels of constant cross section, composed of anisotropic plates each of which can carry any combination of uniformly distributed and longitudinally invariant in-plane stresses. It can be used as either an analysis or an optimum design programme. The analysis principally covers the calculation of eigenvalues, i.e. the critical load factors in elastic buckling problems or the natural frequencies in undamped vibration problems. This analysis is based on the exact solution of the governing differential equations of the constituent members, which are assumed to undergo a deformation that varies sinusoidally, to infinity, in the longitudinal direction, yielding exact stiffness matrices whose elements are transcendental functions of the load factor or frequency and the axial half-wavelength, λ, of the deformation. The resulting transcendental eigenproblem requires an iterative solution which is performed using the Wittrick–Williams algorithm [16]. The simplest form of the buckling analysis [14,15] is performed over a user specified range of values of λ that usually extends from a value less than the smallest plate width to the length, l, of the panel. The lowest buckling load found for any λ is taken as the critical buckling load for the panel. This implies that the panel of length l is simply supported at its ends with warping of the entire cross-section allowed. All results obtained using VICONOPT that are presented in this paper are computed using the VIPASA option [14].

3. Buckling of flat plates with classical boundary conditions

Classical plate theory suggests that a plate will buckle into a mode, where the shape is dependent upon both aspect ratio, applied loading and boundary conditions [17]. Eq. 1 defines the critical stress for an axially loaded plate (of breadth b and length a) resulting in a mode shape made up of a continuous pattern of an integer number of half sine waves (of length λ) in each orthogonal direction, m being the quantity running longitudinally, where $m=a/\lambda_x$ and n transversely $n=b/\lambda_y$.

$$\sigma_{cr} = K\frac{\pi^2 E t^2}{12(1-\upsilon^2)b^2} \tag{1}$$

where K is the buckling coefficient, E is Young's modulus; υ is Poisson's ratio; t is the plate thickness. Fig. 2 shows the buckling coefficient K versus aspect ratio for a flat plate with longitudinal line supports that are both either simply supported or clamped and the loaded edges are simply supported. (A similar figure is presented in ESDU data item 72019 [5]). The lower bound for the simply supported longitudinal plate is the well known result of $K=4$. When the longitudinal edges are clamped the lower bound result increases to $K=6.97$. For a large aspect ratio flat plate it can be then stated that the initial buckling stress will increase by approximately 75% if the longitudinal boundary supports are changed from simply supported to clamped supports.

In ESDU data item 72019 [5] Fig. 2 presents the normalised buckling stress for axially loaded panel with loaded edges simply supported. The longitudinal edges are elastically restrained in rotation, varying from zero elastic restraint to full elastic restraint. When the elastic restraint is zero the longitudinal edge is simply supported and when the elastic restraint is infinite, the longitudinal edge is clamped. The figure then shows the effect of varying the elastic rotational support of plate using the classical boundary conditions as limiting cases.

A stiffened panel is a system of rigidly connected flat plates consisting of a flat skin plate along with a number of stiffeners, each a possible system of thin plates, attached to it. The stiffeners effectively divide the skin plate into a series of long flat strips.

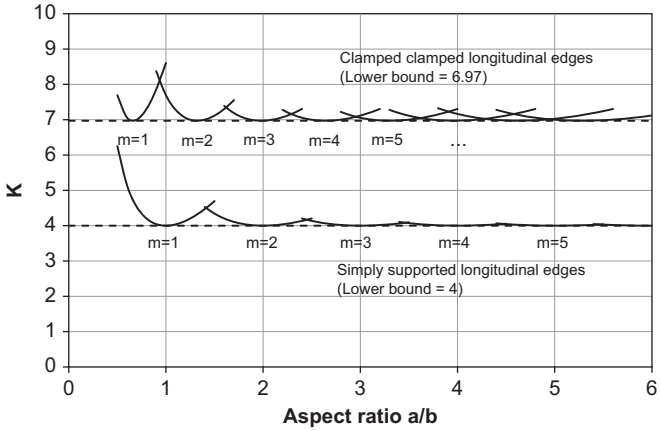

Fig. 2. Buckling coefficient K versus aspect ratio for longitudinally compressed flat rectangular plate. Loaded edges are simply supported. 'm' indicates the number of half-waves along the length of the panel.

The cross section of the stiffened panel investigated in this paper is shown in Fig. 3. The stiffener webs are numbered W1–W6 and the skin portions are numbered P1–P7.

There are six stiffener webs shown in the cross section. The webs then divide the flat square skin into seven long strips. The six line junctions between the stiffener webs and the skin are rigid. A quick method that provides good estimates of initial buckling stresses is to use the approximation that the six line junctions provide boundary conditions akin to simple supports for inter-stiffener portions of skin. A classical simple support does not suppress rotation where as out-of-plane displacement is constrained. In the stiffened panel, shown above, the web of the stiffener is finite in size and therefore only provides a finite, but significant, amount of in-plane stiffness for short wavelength modes of buckling. It also provides some rotational restraint. These two finite non-classical constraints result in constraint in excess of a simple support.

The stiffened panel under consideration is square in plan with length $l=762$ mm. The skin thickness t is 1.27 mm and the stiffener thickness T is 1.473 mm. Stiffener pitch, b_p, is 127 mm; the skin breadth from outermost stiffener (left or right hand side) to support is 63.5 mm and the web breadth, b_w, is 34.34 mm measured to the centreline of the skin. The panel is metal with Young's modulus $E=72.4\,\mathrm{GNm}^{-2}$ and Poisson's ratio $v=0.32$. The longitudinal edges are simply supported and the ends are diaphragm supported. The loading is pure longitudinal compression.

Table 1 shows the predicted, initial buckling stress of the inter-stiffener portion of skin (i.e. the pitch) and web with classical boundary conditions. In the table SS is a simply supported longitudinal edge; C is a clamped longitudinal edge and F is a free longitudinal edge. There are a wide range of buckling half-wavelengths that are considered, from $\lambda=l$ to $\lambda=l/12$. The final column of buckling stresses refers to the actual values of buckling stress computed using VIPASA of the stiffened panel.

In the final column, Table 1 shows that the critical value of stress for the stiffened panel is 31.05 MPa with a buckling half-wavelength $\lambda=l/6$. This mode is skin initiated local buckling between the webs and the corresponding mode has six half-waves down the length. If the longitudinal line junction boundaries between the stiffener webs and skin are idealised so that they are assumed to be simple supports, then each long strip of plate between webs now is a flat plate with an aspect ratio of 6. Fig. 2 above gives $K=4$ for this aspect ratio and the plate has a critical stress of 26.54 MPa (Pitch SS–SS column, $\lambda=l/6$). The web, in the idealised state, has two longitudinal edge boundaries, one edge simply supported and one edge free. The critical stress for the web is 50.70 MPa (Web S–F column,$\lambda=l$) and has a one half-wavelength mode shape. The value for K can be found from Refs. [5–8,17]. In addition a similar figure to Fig. 2 was produced for a plate with one longitudinal edge simply supported/one edge free and a plate with one longitudinal edge clamped/one edge free plate. This figure can be found in Appendix A. NACA technical report 734 [6] presents a similar figure (Fig. 5 in that document) which gives the buckling coefficient of a flat plate of aspect ratio between 0 and 18 with one longitudinal edge free and one longitudinal edge elastically restrained in a range between 0 and infinity on the simply supported edge.

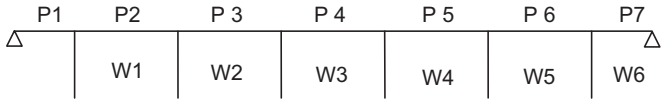

Fig. 3. Stiffened panel cross section.

If the simply supported longitudinal boundaries are now assumed to behave as clamped supports, Table 1 shows the buckling stress increases to 57.08 MPa for the half-wavelength $\lambda=l/6$ (Pitch C–C column) though the critical mode for the inter-stiffener portion of skin (pitch) now has 9 half-waves along the length and critical stress is 46.25 MPa. This value of stress is 74% larger than the critical simply supported result which agrees with the earlier statement above comparing the lower bound results for K based on boundary conditions for long plates. For the web portion the buckling stress at $\lambda=l$ has increased from 50.70 MPa to 7699 MPa (Web C–F column). However the lowest value for web buckling, (not shown in table) is 154 MPa, approximately, at a half-wavelength $\lambda=l/14$. This is an increase by approximately three times which agrees with the ratio of the K values in the limit for long plates (see Appendix A).

The results of Table 1 show that, particularly for the inter-stiffener portion of skin, the line junctions provide more stiffness than the simple supports but someway short of approximating clamped supports.

The mode shapes in Fig. 4 show that rotation is allowed at the line junction and so the line junction is assumed to provide support close to that of a simple support. The initial buckling mode of the panel is a skin initiated buckling mode not a web initiated buckling mode. The results in the table have the longest wavelength $\lambda=l$ with an overall buckling mode and all the other modes are skin initiated local buckling.

Table 1
Classical buckling stresses in MPa of the stiffened panel shown in Fig. 3 with idealised longitudinal boundary conditions at the web and skin line junctions. The analytical results of the whole panel are computed using VIPASA. Critical values for each column are underlined. The loaded edges are simply supported.

Half-wavelength	Component plate				Whole
	P2–P6	P2–P6	W1–W6	W1–W6	panel
λ	SS–SS	C–C	SS–F	C–F	
l	252.3	1243.98	<u>50.70</u>	7699	89.28
$l/2$	73.71	324.07	51.412	1979	77.41
$l/3$	41.46	154.51	52.62	920.8	46.58
$l/4$	31.14	96.11	54.29	551.6	36.18
$l/5$	27.43	70.11	56.45	381.9	32.23
$l/6$	<u>26.54</u>	57.08	59.09	291.1	<u>31.05</u>
$l/7$	27.17	50.38	62.21	237.7	31.40
$l/8$	28.79	47.21	65.81	204.6	32.74
$l/9$	31.14	<u>46.25</u>	69.90	183.3	34.83
$l/10$	34.08	46.80	74.47	169.7	37.52
$l/11$	37.54	48.47	79.53	161.1	40.75
$l/12$	41.46	51.02	85.07	156.3	44.47

4. Buckling modes of stiffened panel

The stiffened panel of Fig. 3 is taken from Ref. [18]. It originates from work done by NASA in 1981. The panel was selected because the axial compression buckling performance was well documented and the panel has been studied by others [19,20]. Although the panel is a thin-walled structure ($b_w/t=100$) the panel itself is not necessarily representative of wing structure where skin thicknesses are larger, as can be seen by the low initial buckling stress as predicted by VIPASA. The mode associated with this buckling stress has a buckling half-wavelength of $\lambda=l/6$. The stress associated with an overall buckling mode (buckling half-wavelength of $\lambda=l$) is 2.875 times the initial buckling stress at 89.28 MPa. This characteristic demonstrates that this panel has stable postbuckling behaviour [19]. The results of the buckling analysis are compared with results obtained using NASTRAN later in the paper. First, however, the buckling mode shapes of the stiffened panel as shown in Fig. 4 are discussed.

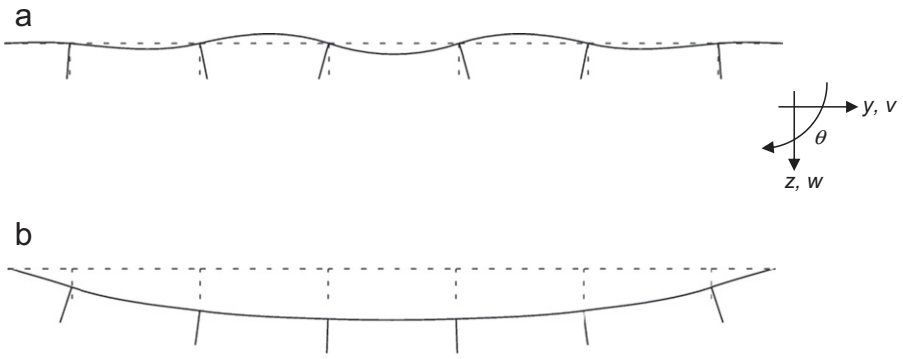

Fig. 4. The computed buckling modes for stiffened panel of Fig. 3. The unperturbed panel is shown dashed. (a) Local mode ($\lambda=l/6$); (b) overall mode ($\lambda=l$)

Table 2
Displacement of longitudinal edges for modes shown. Values normalised to largest value for mode.

Geometry location	Local mode, $\lambda=l/6$			Overall mode, $\lambda=l$		
(See Fig. 3)	v	w	θ	v	W	θ
Top W3	0.000	0.000	1.000	0.000	0.149	0.098
Bottom W3	−0.030	0.000	0.835	−0.004	0.148	0.099
Mid P4	0.000	0.048	0.000	0.000	0.167	0.000

The mode shapes for this stiffened panel fall into two categories that are, as shown, local and overall modes. Local and overall modes can theoretically occur at all wavelengths of buckling although in reality some may not be possible due to material strength considerations. The distinguishing features for each mode can be seen in Fig. 4.

In local modes, the web/skin line junctions do not displace out-of-plane (of the skin) and therefore remain straight. In reality there is some small out-of-plane displacement of the line junction but it is very small in comparison to the displacements of the skin in the centre of each pitch as seen in Fig. 4(a). The magnitude of the out-of-plane displacement is significantly less than one-tenth of the maximum displacement and the statement that the line junction remains straight to the first order accuracy can be made. The free edge of the web is free to displace as can be seen.

For overall modes the longitudinal line junctions between the stiffener webs and the skin do displace out-of-plane and therefore are not straight and, in practice, there is one half wave across the width which looks similar to a half sine wave. Because the panel is simply supported on all edges then the effect is for the stiffeners to bend in-plane for an overall mode. The blades of the stiffened panel have no flanges and so there are no intermediate torsional modes. Torsional modes (or stiffener tripping modes) do exist for flanged stiffeners [20].

The line junction displacements of the stiffener webs with the skin and the free edge of the web are examined here. In Fig. 3 the stiffener webs are numbered from W1 to W6 and skin plates are numbered P1–P7. We could consider all or any web but for the discussion we will examine stiffener web W3 and skin plate P4.

Fig. 4 shows two buckling modes which have very distinguishing features. All the significant displacements of each mode are shown in Table 2. Top W3 refers to the line junction of the web number 3 with the skin and Bottom W3 refers to the free edge of stiffener web number 3. Mid P4 refers to the midpoint of the skin plate P4. The displacements of each node are normalised with respect to the maximum displacement in that mode. Note that the longitudinal displacements are negligible and are ignored and that out-of-plane displacements for the skin are in the z axis direction and out-of-plane displacements for the web are in the y axis direction.

For the local mode, the rotation of the line junction (about the x axis) is the largest displacement (Top W3 $\theta=1.000$). There is also some lateral displacement (out-of-plane) of the free edge of the web in the y axis direction (Bottom W3 $v=-0.030$). The rotation of Bottom W3 is slightly lower ($\theta=0.835$) showing a small amount of bending of the web plate thus suggesting some rotational restraint being provided by the support. The numerical data shows no out-of-plane or in-plane displacement at Top W3 to the accuracy stated. Mid P4 shows an out-of-plane displacement of $w=0.048$. This shows that the local mode is precipitated by the buckling of this portion of structure because it has the largest value. The overall mode shows both rotation and out-of-plane displacement at both edges of the web plate (Top W3 $w=0.149$ and Bottom W3 $v=-0.004$) and out-of-plane displacement at the midpoint of skin plate P4 $w=0.167$. Note the largest displacement for the overall mode is rotation at the free edge of web W1, i.e. Bottom W1 $\theta=1.000$).

The local mode displacements show then that the line junctions remain straight and rotate only. There is some small degree of rotational restraint provided. The addition of the filleted junction adds material to the line junction location. This material then can provide further restraint against rotation and hence can change the tendency of the line junction behaviour away from that of a simple support towards that of a clamped support in the limit.

5. Cross section geometry

This section of the paper presents the properties of the cross sections for each of the models for both the analytical and numerical models. The analyses carried out in this paper, have utilised a finite strip model (using VIPASA) which uses 2D strip elements; a 2D Finite Element model (NASTRAN) and 3D Finite Element models (NASTRAN). The 2D element models assume a thickness for each element, hence when constructing a 2D model of a stiffened panel the 2D elements will overlap at the line junctions of stiffener webs and skin (and webs with flanges in the case of more complex stiffener arrangements).

This overlap can be compensated for by offsetting elements by an appropriate amount and then use rigid beam elements to link the offset elements. A study for the stiffened panel showed that the extra accuracy obtained by using offsets was small and so for this paper the overlap was allowed and offsets were not used. One consequence of this overlap is that the area of overlap is double counted. This is shown in Table 3 that shows the 2D element model has a cross sectional area of 1271 mm^2 and is a larger area than the 3D square junction model which has a cross sectional area of 1266 mm^2. This overlap then is small (0.44% difference)

Table 3
Geometrical properties of cross section of panel. Percentage values are compared to 3D square junction results shown in column 3. Neutral axis position is given relative to outside of skin away from webs.

Geometry Property	2D	3D (square)	3D ($r=1$)	3D ($r=2$)	3D ($r=3$)	3D ($r=4$)	3D ($r=5$)
Area mm^2	1271	1266	1268	1276	1289	1307	1330
% area increase	0.44	–	0.20	0.81	1.83	3.26	5.09
2nd Moment of area (mm^4)	98,067	97,986	98,014	98,080	98,164	98,247	98,317
% 2nd Moment increase	0.082	–	0.028	0.095	0.181	0.266	0.337
Neutral axis (mm)	4.099	4.751	4.744	4.726	4.700	4.669	4.637

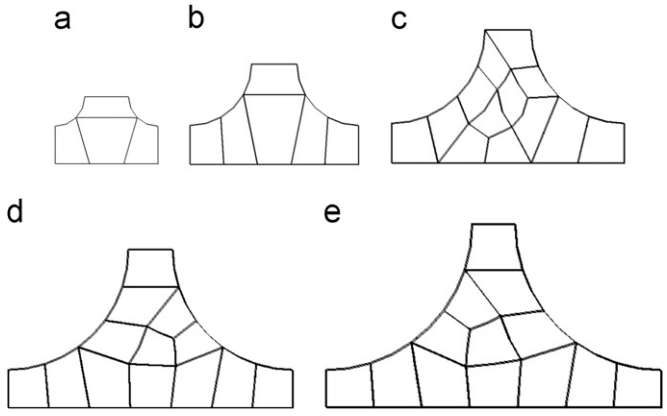

Fig. 5. Cross sections of the 5 filleted junctions for the finite element analysis. The cross sections show only the filleted portions of the junction. (a) $r=1$ mm; (b) $r=2$ mm; (c) $r=3$ mm; (d) $r=4$ mm; (e) $r=5$ mm. The web thickness is 1.473 mm therefore in (e) 5 mm fillet model has a total width of 11.473 mm

and as stated does not significantly affect the numerical values of critical load.

Fig. 1 shows the junction of a web with the skin for the filleted 3D model and square junction 3D model. The geometrical properties of cross sectional area; 1st moment of area; 2nd moment of area; and vertical position of the neutral axis for all the 2D and 3D models are given in Table 3. All these properties are affected by the presence and size of the filleted junctions. These calculations and the theory for the geometrical properties of the fillets are shown in Appendix B. A survey of the mathematical literature did not reveal the calculation of 2nd moment of area of one fillet portion around its local axis which is shown to be (see Appendix B)

$$I_0 = r^4[(1-\frac{5\pi}{16})-(1-\frac{\pi}{4})\frac{(10-3\pi)^2}{(12-3\pi)^2}] \quad (2)$$

The area increases to a maximum of 5.09% for the 5 mm radius model compared to the 3D square junction model and the second moment of area for the 5 mm model only shows a 0.337% increase. Fig. 5 shows the FE cross section of the junctions of the web with the skin for the fillet range of $r=1$–5 mm. The cross sections are not drawn to scale however their relative sizes are approximately correct. Pictorially it is seen that there is significantly more material at the line junction for the $r=5$ mm model compared to the $r=1$ mm model which would suggest more stiffness, leading to higher buckling loads for those modes that are influenced by the line junctions such as local modes. In Section 6 this is quantitatively expressed. With regard to the second moment of area the small increase of 0.337%, over the range from square junction to radius 5 mm fillets, is as a result of the additional area being added at the web skin junction which is close to the neutral axis of the section.

6. Finite element modelling

Three different finite element models, using MSC NASTRAN [9], were produced. Initially a two dimensional (2D) element model of the stiffened panel in Fig. 3 was produced using CQUAD4 [9] elements. The CQUAD4 element is a quadrilateral element with 4 nodes. A buckling analysis was carried out to determine the buckling loads of the different wavelengths and these were compared with the VIPASA results in Table 4. A three dimensional (3D) element model was then created with a square junction and the buckling analysis of this panel is also shown in Table 4 using CHEXA solid elements. The CHEXA element is a solid element with 6 faces and up to 20 nodes and HEX20 is used throughout to denote the use of these solid elements with 20 nodes made up of 8 corner nodes and 12 mid-edge nodes. The third model was the 3D element model with the range of fillet radii shown in Table 4 with radii varying from 1 mm to 5 mm. The VIPASA results are exact analytical results. The finite element results are numerical solutions.

6.1. 2D finite element model

The finite element models were loaded using displacement control. The panel is simply supported so out-of-plane displacement, $w=0$, was applied to nodes on the four edges of the skin portion of the panel as shown in Fig. 6(a). With the position of the neutral axis already calculated one node was created and positioned centrally on that axis at each end of the panel as shown in the figure by the two circles shown solid. Two Rigid Body Elements (type RBE2), one at each end of the panel, linked the new nodes (independent nodes) to all nodes on that panel cross section end (dependent nodes) respectively forming a multipoint constraint (MPC), as seen in Fig. 6(b). (Note this figure shows a coarse mesh which is used to show the application of the RBE. A mesh sensitivity analysis was carried out to ensure converged numerical results which resulted in a higher mesh element density). Displacement, u, in the x direction for all the dependent nodes was linked to the independent created node. This allowed for panel cross section rotation at the supports about the neutral axis.

Load was applied to the panel by applying a unit displacement, $u=1$, to the created node in the x direction as indicated in Fig. 6(a). The respective node at the opposite end of the panel was constrained in the x direction to have zero displacement, $u=0$, along the x axis. One longitudinal line of nodes in the skin had zero in-plane transverse displacement ($v=0$) to allow for Poisson's effect and all nodes at each end of the web were constrained to have zero rotation about the x axis.

Table 4
Buckling stress values in MPa using VIPASA, 2D FE, 3D FE square and fillet junctions of stiffened panel. (Critical values are underlined.)

Half-Wave length λ	VIPASA no. Offsets	2D CQUAD4 no. Offsets	3D HEX20 square	3D HEX20 radius 1 mm	3D HEX20 radius 2 mm	3D HEX20 radius 3 mm	3D HEX20 radius 4 mm	3D HEX20 radius 5 mm
l	89.28	94.47	96.28	96.54	95.90	95.57	94.46	93.25
$l/2$	77.41	78.87	79.49	80.37	81.37	83.95	87.38	92.84
$l/3$	46.58	46.70	47.33	48.00	48.99	51.29	54.53	59.49
$l/4$	36.18	36.11	36.76	37.35	38.31	40.42	43.43	47.88
$l/5$	32.23	32.05	32.75	33.30	34.21	36.17	38.91	42.85
$l/6$	31.05	30.83	31.57	32.10	32.96	34.78	37.25	40.70
$l/7$	31.40	31.17	31.94	32.45	33.26	34.85	37.17	40.18
$l/8$	32.74	32.54	33.32	33.82	34.57	36.14	38.13	40.78
$l/9$	34.83	34.71	35.45	35.95	36.65	38.02	39.90	42.27
$l/10$	37.52	37.56	38.20	38.69	39.35	40.72	43.74	44.38

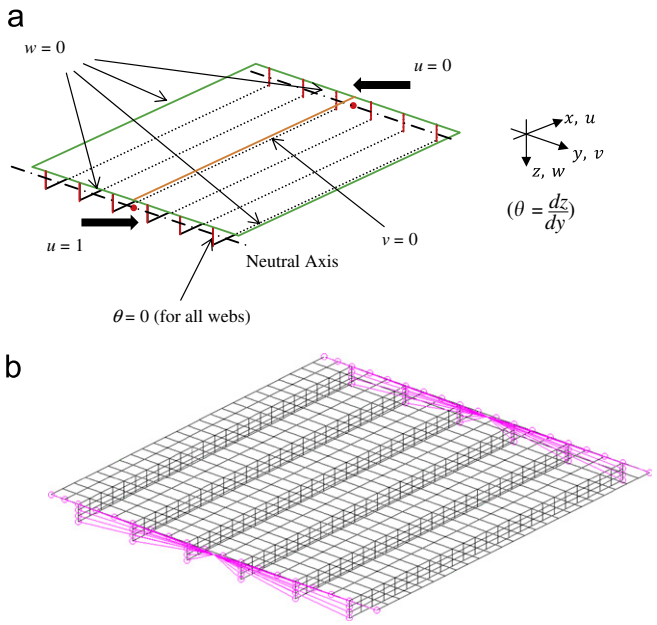

Fig. 6. (a) Loading and boundary conditions applied to panel. Loading applied using displacement method and (b) RBE element used to link all nodes on cross section at each end of the panel to node created on neutral axis.

To keep the webs straight, at each end an RBE2 element was used for each web to link the out-of-plane transverse displacement, v. A node in the skin at the junction with each web was used as the independent node and the nodes on each web were the dependent nodes for each RBE2 elements applied to the web nodes. These Rigid Body Elements allowed the webs to displace laterally and remain straight whilst the rotation constraint on the webs ensured the webs remained vertical.

The buckling stress results for the 2D elements, shown in Table 4, compare very well with the analytical results from VIPASA over the whole range of half wavelengths. For $\lambda = l$ the result is high compared to the VIPASA result, 94.47 MPa compared to 89.29 MPa. This results from the fact that VIPASA allows for warping of the cross section and the FE model does not allow for cross section warping at the ends. Use of Rigid Body Elements has caused a small increase in stiffness at the loaded edges resulting in a larger overall buckling stress

6.2. 3D finite element model.

In the same way as the 2D model, the 3D finite element models were loaded using displacement control. The position of the neutral axis was calculated and again two extra nodes were created and positioned centrally on the neutral axis, one at each end of the loaded panel. One node was displaced in the longitudinal direction and the other node was constrained to have zero displacement. Solid HEX20 elements were used and these elements have mid nodes on each element edge.

The constraints used for the 3D model were very similar to those used for the 2D model shown in Fig. 6(a). If Fig. 6(a) is viewed as a mid-plane model of the 3D element model then the figure shows the constraints that are applied to that 3D model; the mid-plane model being the plane at the mid-thickness of the component plates. So for the skin elements, only the nodes on the edges of the skin mid-plane were constrained for out of plane displacement. Poisson's effect was allowed by constraining one longitudinal line of skin mid-plane nodes only to have zero in-plane-transverse displacement.

For each web in turn, all the mid-plane nodes of that plate, at each end of the panel, were constrained using an MPC and the nodes connected using a rigid body element (RBE2). The MPC is used to link the transverse displacement, v, in the y direction on the nodes of the web at each end as on the 2D model. The independent node was selected as a node in the skin that was in line with the web. For all nodes on the mid-plane at each end of the webs, zero rotation about the x axis was imposed. As for the 2D model, the RBEs ensured the webs remained straight and were allowed to displace laterally while the rotation constraint ensured the webs remained vertical.

As for the 2D model, to model the simple supports at the loaded end in the 3D model, multiple point constraints were also used. At each loaded end, the independent node was the node created on the neutral axis and all nodes on the mid-plane of the cross section were linked as dependent nodes with displacement in the longitudinal direction linked to the independent node via a rigid body element (RBE2). This allowed for cross section panel rotation about the neutral axis. The results for the 3D element square junction compared very well with the 2D element result as can be seen in Table 4.

6.3. 3D finite element model with filleted junctions.

This model is in essence very similar to the 3D square junction panel. The only difference is the line junction between the web and skin that has the presence of a fillet. The junctions were meshed using the 'Paver' option in PATRAN. Fig. 5 shows the cross section of the 5 filleted junctions as meshed using PATRAN.

Table 4 shows that while critical buckling stresses rises with an increase in fillet radius, the critical buckling mode occurs at a shorter half-wavelength. For fillet radius of 4 mm and 5 mm the critical mode has a half-wavelength $\lambda = l/7$ compared to $\lambda = l/6$ modes for the other models.

Table 5
Buckling load in *N* for the stiffened panel under investigation. The % increase values are compared to the square junction result.

Buckling	2D	3D	3D	3D	3D	3D	3D
Mode		(square)	(r=1)	(r=2)	(r=3)	(r=4)	(r=5)
Overall	120,088	121,850	122,436	122,357	123,176	123,447	124,024
% increase	−1.45		0.48	0.42	1.09	1.31	1.78
Local	39,198	39,957	40,708	42,050	44,819	48,575	53,445
% increase	−1.90		1.88	5.24	12.17	21.57	33.76

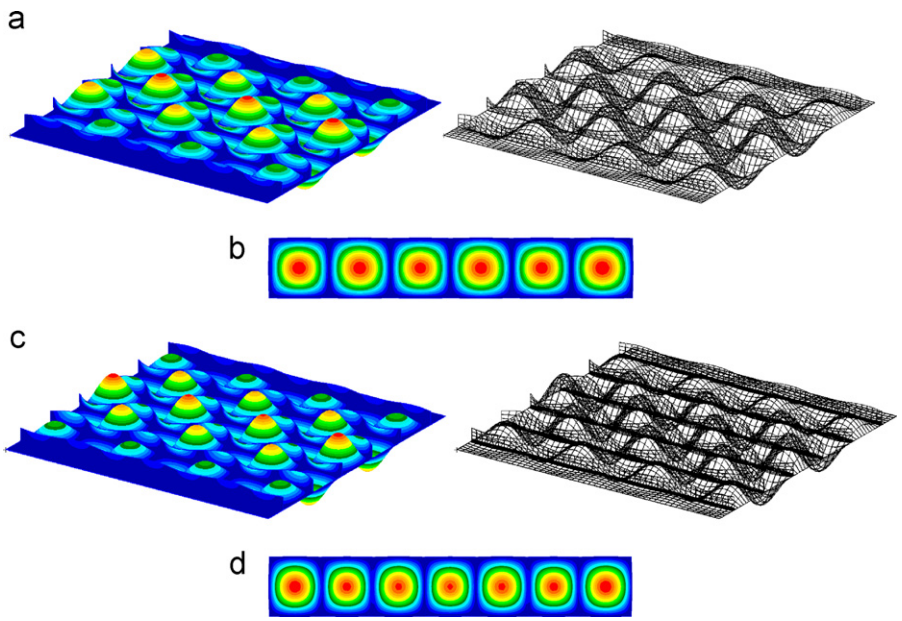

Fig. 7. Critical buckling mode shapes for Square junction panel and Fillet radius r=5 mm panel. (a) Whole panel (Square junction); (b) central skin plate P4of Square junction panel; (c) whole panel (Filler radius=5 mm); (d) central skin plate P4 (fillet radius r=5 mm panel).

The overall buckling stress varies from 96.54 to 93.25 MPa for the solid models. Although the stress values reduce with increasing radius from r=1 mm to r=5 mm, due to the area increases, the actual buckling loads have increased. The local buckling stress values have increased, across the range of radii, and when expressed as buckling load the percentage values are larger compared to the stress results. This is shown in Table 5, below, which shows the predicted buckling loads associated with the overall mode at half wavelength $\lambda=l$ and the critical local skin buckling.

Table 5 shows that the r=5 fillet junction panel has an initial buckling load that is 33.76% greater than the initial buckling performance of the square junction panel. This compares to a 27.28% difference in the stress value comparison. The overall buckling stress for the 5 mm model is 93.25 MPa compared with 96.28 MPa for the square model, which is a 3.1% decrease. The overall buckling load shows a 1.78% increase compared to the square junction result for the overall mode. The performance gains from the fillet junction in terms of initial buckling are very significant when compared to the mass penalty i.e. a 33.76% increase in initial buckling load versus a 5.09% increase in mass.

Fig. 7 shows the change in mode shape for the critical modes for the square junction panel model and the fillet radius r=5 mm panel model. Fig. 7(a) shows the complete panel with square junctions buckling at $\lambda=l/6$. Fig. 7(b) shows the central plate P4 (see Fig. 3) only. It shows a very similar mode to classical mode of a plate of aspect ratio a/b=6 with simple supports longitudinally. Fig. 7(c) shows the complete panel with fillet radius r=5 mm at the web/skin line junction. The mode shown has seven half-waves down the length which is more easily seen in Fig. 7(d). Fig. 7(d) shows the central plate P4 buckling with a half wavelength $\lambda=l/7$.

Table 6
Effective *K* values for: flat plate and inter-stiffener portions of skin for NASA panel. The final row gives buckling half-wavelength, λ.

Plate	VIPASA	Square	r=1	r=2	r=3	r=4	r=5
Aspect ratio 6		junction					
4	4.68	4.76	4.84	4.97	5.24	5.60	6.06
$l/6$	$l/6$	$l/6$	$l/6$	$l/6$	$l/6$	$l/7$	$l/7$

It is known that the buckling coefficient *K* is dependent on the boundary conditions of the plate [5]. ESDU data item 72019 [5] presents data sets for a range of elastically restrained, in rotation, longitudinal edges. The results presented herein enable the computation of a similar set of results for component plates of stiffened panels. If it is known which component plate initiates local buckling then it will be possible to calculate a buckling coefficient as a function of the line junction geometry. For the panel investigated in this paper it is the inter-stiffener portion of

skin that initiates the buckling. Table 6 presents effective '*K*' values for this inter-stiffener portion of skin. For the idealised case a simply supported plate has $K=4$. For the square junction version of the panel K value is of 4.68. The addition of the 5 mm radius fillet junction raises the K value to $K=6.06$. Table 6 also shows the buckling half-wavelength of the critical mode.

7. Conclusions

It is well known that the line junction between component parts of a stiffened panel provides finite displacement and rotational stiffness. The combination of these two effects is such that simple supports can be conservatively assumed at the line junction between stiffener webs and inter-stiffener portions of skin. For the stiffened panel investigated in this paper a buckling coefficient value for the line junction, with fillet radius 5 mm, was calculated as $K=6.06$. The lower bound idealised value is $K=4$ for longitudinal simple supports and the upper bound is $K=6.97$. The suggestion is therefore that there is a practical limit to simply adding mass at line junctions to increase local buckling stability. However, by taking account of the fillet in the numerical analysis it is shown that the line junction provides more stiffness shown by the increase in critical buckling stress where the fillet is assumed to result from the manufacturing process e.g. machining or extrusion. The authors suggest that a fillet size leading to a value of K greater than the upper bound value would be an over-sized fillet.

Aerospace engineers tend to use load per unit width of the panel. The results have shown that local buckling stability has increased by 34%. Since the skin thicknesses of the filleted and non-filleted geometry are identical at $t=1.27$ mm then percentage value also applies to load per unit width. The study shows that the stiffened panel with a fillet radius of 5 mm has an initial buckling stress of 40.18 MPa compared to the square junction result of 31.57 MPa. Due to the area change the actual difference in load is larger than that the stress values immediately suggest. The classical stress values for the inter-stiffener portion of skin vary from 26.54 MPa with simple supports longitudinally to 46.25 MPa with clamped supports longitudinally. Interestingly the numerical model shows the critical buckling mode also changed with increasing fillet radius at $r=4$ mm. This is an expected result if Fig. 2 and Table 1 are examined carefully. For plates with classical boundary conditions with an aspect ratio of $a/b=6$ and longitudinal simple supports the critical mode has half-wavelength $\lambda_{crit}=l/6$. For clamped longitudinal supports the critical mode has half-wavelength $\lambda_{crit}=l/7$. The fillet radius at the line junction provides a non-classical boundary support lying in between simple support and clamped. For the results with fillet radius $r=4$ mm and $r=5$ mm the critical modes have half-wavelength $\lambda_{crit}=l/7$ which lies between the lower bound of half-wavelength $\lambda_{crit}=l/6$ and the upper bound half-wavelength $\lambda_{crit}=l/9$.

The panel investigated has a low buckling stress as compared to realistic sized aerospace panels. However the results clearly show that filleted junctions do alter the local buckling behaviour of stiffened panels. Since the panel did not have flanged stiffeners the neutral axis location and fillet junction were close resulting in small increases in overall buckling stability. It is therefore important for panel designers to take account of this extra stiffness provided by filleted line junctions and use this knowledge in improving panel buckling stability. Filleted junctions can also lead to lower mass panels if designers reduce the area of the cross section because of the increased stability.

Boundary conditions greatly influence overall buckling behaviour and less so local buckling behaviour. The result for overall buckling for the numerical model was higher compared to the analytical results of VIPASA. This difference was due to the numerical model not allowing warping of the cross section as compared to VIPASA which does allow warping. All the stress values for the local modes ($\lambda \geq l/2$) for the square junction model showed very good comparison to the VIPASA results as they are less affected by the panel boundary conditions.

The paper has not examined postbuckling behaviour but for the panel examined the extra area located close to the neutral axis of the section results in a panel with only a negligible increase in overall buckling load. Hence the postbuckling behaviour would be influenced significantly by the presence of a filleted line junction. Further work should also include flanged stiffened panels.

Acknowledgements

The authors wish to thank the Engineering and Physical Sciences Research Council and Airbus U.K. for providing the financial assistance that made this work possible. In addition they would like to thank Rohan Vashisht, an undergraduate in the Aeronautical and Automotive Engineering Department at Loughborough University, for his help and advice in using the post-processing features of PATRAN and Hausigan Sivayogarajah for his contribution to this work with his undergraduate project under the supervision of the second author.

Appendix A

Fig. A1.

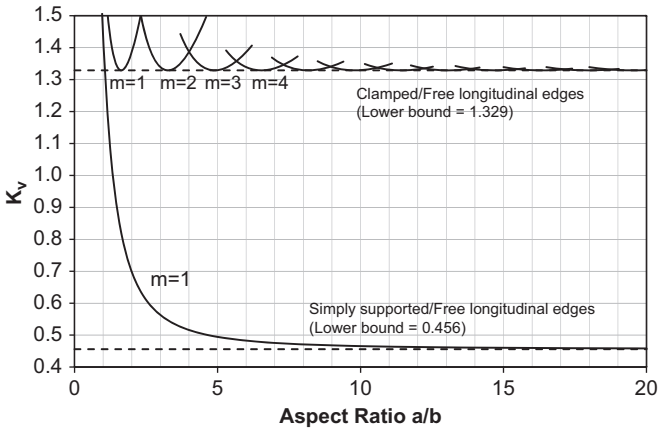

Fig. A1. Buckling Coefficient K_V for uniformly compressed flat rectangular plate, length a and breadth b, with different aspect ratios for two sets of longitudinal line supports indicated. 'm' indicates the number of half waves along the length of the panel. Loaded edges are simply supported. Poisson's ratio is 0.25.

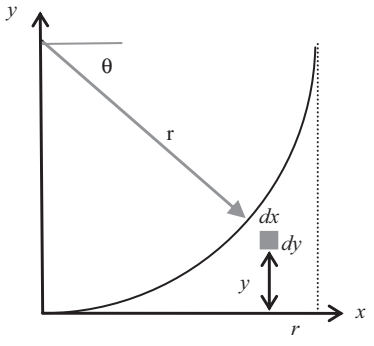

Fig. B1. Cross section of fillet and elemental area.

Appendix B

B1. Area of the fillet

Consider the area under the curve in Fig. B1. The equation for the curve is

$$x^2+(y-r)^2=r^2$$

Area, A, under the curve between the limits of $x=0$ and $x=r$

$$A=\int dA=\int\int dxdy=\int_0^r\int_{[r^2-(y-r)^2]^{1/2}}^{r} dxdy=\int_0^r [x]_{[r^2-(y-r)^2]^{1/2}}^{r} dy$$

Changing to polar coordinates and using the following substitutions

$$y=r-r\sin\theta;\quad x=r-r\cos\theta;\quad dy=-r\cos\theta\, d\,\theta$$

Area A under the curve is then calculated as

$$A=\int_{\pi/2}^{0}[x]_{r\cos\theta}^{r}(-r\cos\theta)d\theta=\int_0^{\pi/2}(r-r\cos\theta)r\cos\theta\, d\,\theta$$
$$=r^2\int_0^{\pi/2}(\cos\theta-\cos^2\theta)d\,\theta=r^2\int_0^{\pi/2}(\cos\theta-\frac{\cos 2\,\theta+1}{2})d\theta$$
$$=r^2[\sin\theta-\frac{\sin 2\theta}{4}-\frac{\theta}{2}]_0^{\pi/2}=r^2(1-\frac{\pi}{4})$$

B2. First moment of area of the fillet

Consider the elemental strip shown in Fig. B2 obtained by integrating the elemental area dA with respect to x. The position of the neutral axis of the area under the curve measured to the x axis is defined as $\bar{y}$. To calculate $\bar{y}$ we need the 1st moment of area about the x axis given as

$$\bar{y}\int dA=\int ydA=\int yxdy$$

In polar notation with the above substitutions

$$\int yxdy=\int_0^{\pi/2}(r-r\sin\theta)(r-r\cos\theta)r\cos\theta\, d\,\theta$$
$$=r^3\int_0^{\pi/2}(\cos\theta-\sin\theta\cos\theta-\cos^2\theta+\sin\theta\cos^2\theta)d\,\theta$$
$$=r^3[\sin\theta+\frac{\cos 2\theta}{4}-\frac{\sin 2\theta}{4}-\frac{\theta}{2}-\frac{\cos^3\theta}{3}]_0^{\pi/2}$$
$$=r^3(\frac{5}{6}-\frac{\pi}{4})=.2234r$$

The above result can be obtained by using the known results for a square and quadrant and subtracting. The position of neutral axis is then given as

$$\bar{y}=\frac{\int ydA}{\int dA}=\frac{r^3(\frac{5}{6}-\frac{\pi}{4})}{r^2(1-\frac{\pi}{4})}=\frac{r(10-3\pi)}{(12-3\pi)}$$

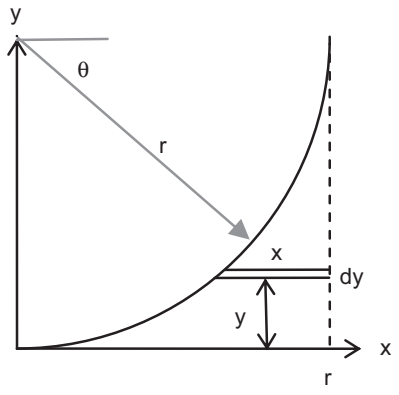

Fig. B2. Cross section of fillet and elemental strip of area.

B3. Second moment of area of the fillet

The second moment of area, I, about the x axis can be calculated as follows:

$$I=\int y^2dA=\int_0^r y^2xdy$$

In polar notation with the above substitutions

$$I=\int_0^{\pi/2}(r-r\sin\theta)^2(r-r\cos\theta)r\cos\theta d\theta$$
$$=r^4\int_0^{\pi/2}(1-2\sin\theta-\sin^2\theta)^2(1-\cos\theta)\cos\theta d\theta$$
$$=r^4\int_0^{\pi/2}(\cos\theta-2\sin\theta\cos\theta+\cos\theta\sin^2\theta-\cos^2\theta$$
$$+2\sin\theta\cos^2\theta-\cos^2\theta\sin^2\theta)d\theta$$

Now

$$-\cos^2\theta\sin^2\theta\rightarrow\quad-\cos^2\theta(1-\cos^2\theta)\quad\rightarrow\quad-\cos^2\theta+\cos^4\theta$$

$$I=r^4\int_0^{\pi/2}\cos\theta-\sin 2\theta+\cos\theta\sin^2\theta-1+2\sin\theta\cos^2\theta$$
$$+\frac{\cos 4\theta}{8}-\frac{\cos 2\theta}{2}+\frac{3}{8}d\theta=r^4\left[\sin\theta+\frac{\cos 2\theta}{2}+\frac{\sin^3\theta}{3}-\frac{\sin 2\theta}{2}\right.$$
$$\left.-\theta-\frac{2\cos^3\theta}{3}+\frac{\sin 4\theta}{32}-\frac{\sin 2\theta}{4}+\frac{3\theta}{8}\right]_0^{\pi/2}=r^4(1-\frac{5\pi}{16})$$

Using parallel axes theorem

$I=I_0+Ay^2$ where I_o is the second moment of area about local axis

We have established that

$$\bar{y}=\frac{r(10-3\pi)}{(12-3\pi)};\quad I=r^4\left(1-\frac{5\pi}{16}\right);\quad A=r^2\left(1-\frac{\pi}{4}\right)$$

Hence $I_0=I-Ay^2$

$$I_0=r^4[(1-\frac{5\pi}{16})-(1-\frac{\pi}{4})\frac{(10-3\pi)^2}{(12-3\pi)^2}]=0.007545116r^4$$

We considered only the fillet joining the web to the skin. If there are flanges to consider then the fillet area will become inverted. This is not an issue since we now have the local value and only need to know y value to neutral axis of section.

References

[1] Hutchinson JW, Koiter WT. Postbuckling theory. Applied Mechanics Reviews 1970;23:1353–66.
[2] Munroe J, Wilkins K, Gruber M. Integral Airframe Structures (IAS)—validated feasibility study of integrally stiffened metallic fuselage panels for reducing manufacturing costs. NASA Contractor Report. NASA/CR-2000-209337; May 2000.
[3] Quinn D, Murphy A, McEwan W, Lemaitre F. Stiffened panel stability behaviour and performance gains with plate prismatic sub-stiffening. Thin-Walled Structures 2009;47:457–1468.
[4] Fenner PE, Watson A. Approximate analysis of filleted junction stiffened plates using finite strip method. In: Proceedings of ICTWS 2008 international conference on thin-walled structures; June 2008. p. 163–9.
[5] ESDU Data Sheet 72019. Buckling of flat isotropic plates under uniaxial and biaxial loading; 1972.
[6] Lundquist EE, Stowell EZ. Critical compressive stress for outstanding flanges. NACA Technical Report no. 734; 1942.
[7] Hill HN. Chart for critical compressive stress of flat rectangular plates NACA Technical note no. 773; 1940.

[8] Gerard G, Becker H. Handbook of structural stability part I: buckling of flat plates. NACA Technical note no. D-162; 1957.
[9] Taylor R. The role of optimization in component structural design: application to the F-35 joint strike fighter, 25th International Congress of the Aeronautical Sciences; 2006.
[10] Quinn D, Murphy A, Cervi L. Fatigue performance of aircraft panels with novel skin buckling containment features. in: Proceedings of the institution of mechanical engineers, part G: Journal of Aerospace Engineering, vol. 225; 2011.p. 791.
[11] Lillico M, Butler R, Hunt G, Watson A, Kennedy D, Williams FW. Analysis and testing of a postbuckled stiffened panel. American Institute of Aeronautics and Astronautics Journal 2002;40(5):996–1000 ISSN 00011452.
[12] Williams FW, Kennedy D, Butler R, Anderson MS. VICONOPT: program for exact vibration and buckling analysis or design of prismatic plate assemblies. American Institute of Aeronautics and Astronautics Journal 1991;29(11): 1927–8.
[13] MSC. Software (2004). MSC. Nastran 2001 Users Guide. MSC. Software.
[14] Wittrick WH, Williams FW. Buckling and vibration of anisotropic or isotropic plate assemblies under combined loadings. International Journal of Mechanical Sciences 1974;16(4):209–39.
[15] Anderson MS, Williams FW, Wright CJ. Buckling and vibration of any prismatic assembly of shear and compression loaded anisotropic plates with an arbitrary supporting structure. International Journal of Mechanical Sciences 1983;25(8):585–96.
[16] Wittrick WH, Williams FW. A general algorithm for computing natural frequencies of elastic structures. Quarterly Journal of Mechanics and Applied Mathematics 1971;24(3):263–84.
[17] Timoshenko SP, Gere JM. Theory of elastic stability. 2nd edition. McGraw Hill; 1961.
[18] Stroud WJ, Greene WH, Anderson MS. Buckling loads for stiffened panels subjected to combined longitudinal compression and shear loadings: results obtained with PASCO, EAL, and STAGS Computer Programs. NASA Technical report no. 83194; 1984.
[19] Dawe DJ, Wang S. Postbuckling analysis of composite laminated panels. American Institute of Aeronautics and Astronautics Journal 2000;38.
[20] Watson A, Fenner PE, Featherston CA, Kennedy D. Postbuckled stability of panels with torsional buckling. In: Proceedings of the 50th AIAA/ASME/ASCE/AHS/ASC, structures, structural dynamics and materials conference; May 2009. p. AIAA 2009-2510.